European Journal of Inorganic Chemistry

EurJIC
European Journal of Inorganic Chemistry

Chemistry Europe
European Chemical Societies Publishing

RESEARCH ARTICLE OPEN ACCESS

Switchable Dual Emission of Luminescent Metal–Organic Framework@Nanoparticle Composites of EuBDC and ZrO-Containing Hybrid Materials

Tobias Wehner[1] | Joachim G. Heck[2] | Claus Feldmann[2] | Klaus Müller-Buschbaum[1,3]

[1]Institute of Inorganic and Analytical Chemistry, Justus-Liebig-University Giessen, Giessen, Germany | [2]Institute of Inorganic Chemistry, Karlsruhe Institute of Technology (KIT), Karlsruhe, Germany | [3]Center for Materials Research (LAMA), Justus-Liebig-University Giessen, Giessen, Germany

Correspondence: Klaus Müller-Buschbaum (klaus.mueller-buschbaum@anorg.chemie.uni-giessen.de)

Received: 21 May 2026 | **Revised:** 14 July 2026 | **Accepted:** 16 July 2026

Keywords: composites | dual emission | luminescence | metal–organic frameworks | nanoparticles

ABSTRACT

For the preparation of luminescent materials with dual emission that combine two different luminescence processes with reversible switchability, the Eu^{3+}-containing metal–organic framework (MOF) $^{3}_{\infty}[Eu_2(BDC)_3]\cdot 2DMF\cdot 2H_2O$ (EuBDC) (BDC = benzene dicarboxylate) was combined with zirconyl-containing nanoparticles ZrO(FMN) (FMN = flavin mononucleotide) and ZrO(MFP) (MFP = methyl fluoresceinphosphate), respectively. The resulting composite materials form dispersions in various media and combine the green luminescence of the nanoparticles with the red luminescence of the Eu^{3+}-containing MOF. Switching between the different chromaticities is enabled without a chemical transformation of the emitter but by variation of the excitation wavelength, as the emission processes of the two composite components exhibit different excitation wavelengths. While the FMN-containing composite particles own a red/green luminescence, the chromaticity of the MFP-containing system is further influenced by a strong solvatochromic effect of the nanoparticles. Therefore, further luminescence colors that comprise a large part of the visible spectrum can be generated in dependence of the solvent/dispersion media.

1 | Introduction

Stimuli-responsive compounds, also called smart materials, have gained enormous interest in science and technology in recent years [1–9]. Such materials undergo changes in certain properties after variation of an external condition. For instance, physical or chemical stimuli like temperature [10–14], light irradiation [15–20], magnetic changes [21–23], voltage [24], or pH value [25–29] can induce a change of properties.

Particularly light-responsive materials have gained attention in the field of stimuli-responsive materials [1, 2, 18, 19, 30–32]. Optical switchable smart materials can, for instance, be used as biomarkers for in vivo detection in various biomedical procedures like protein tracking [33–35], fluorescence resonance energy transfer imaging [36–39] or imaging of hydrogen peroxide [40]. For this purpose, different photo-switchable fluorescent proteins can be applied [33–39]. Other fields of application for photo-switchable materials are rewritable data storages [41, 42], optical switches [43] and chemical sensors [44]. For these applications, mostly photochromic materials are used. These materials can change their physical properties like transmission, reflection, or fluorescence after a photochemical reaction [41, 42, 45]. A huge variety of materials like carbocyanine dyes [46], spiropyran-based polymer nanoparticles [47], Eu^{3+}-containing metal–organic frameworks (MOFs) [48] or EuSiWMo/agarose composite films [49] can be applied as photochromic switches. Multimaterial MOF patterning is possible by inks from MOF crystal suspensions [50].

Especially, lanthanide-containing MOFs exhibit remarkable optical properties enabling sensing of chemical and physical changes,

which are mostly based on changes of their luminescence [51–53]. Amongst them, the series of lanthanide-containing MOFs featuring different lanthanide ions and benzene dicarboxylate as linker (LnBDC), with the europium-variant being most prominently investigated [54–56].

However, several systems for photochromic switching have the disadvantage that the luminescence change of the material is accompanied by a photochromic structural change that is irreversible, leading to an explicitly limited use as photochromic systems [34, 35]. To address this, we generated the composite materials $^{3}_{\infty}[Eu_2(BDC)_3]\cdot 2DMF\cdot 2H_2O$@ZrO(FMN) (EuBDC@ZrO(FMN) (**1**), with FMN = flavin mononucleotide, BDC = benzene dicarboxylate) and $^{3}_{\infty}[Eu_2(BDC)_3]\cdot 2DMF\cdot 2H_2O$@ZrO(MFP) (EuBDC@ZrO(MFP) (**2**), with MFP = methyl fluoresceinphosphate) as optical switchable materials. Due to their two-component character, the composite materials described in this report enable a reversible switching between the luminescence of the Eu^{3+}-containing MOF and of the nanoparticles just by variation of the excitation wavelength. Only very few examples of reversible switchable materials have been reported in literature so far, including fluorescent proteins and spiropyran-based polymer nanoparticles [47, 57, 58].

2 | Results and Discussion

The inorganic–organic hybrid materials ZrO(FMN) and ZrO(MFP) were selected as starting components for the MOF-functionalized multi-luminescent composite particles. Nanoparticles of the type $[ZrO]^{2+}[R_{dye}OPO_3]^{2-}$ can be synthesized by a one-pot reaction of $ZrOCl_2$ with sodium salts of the particular dyes. The particles show a diameter of 30–40 nm, form stable colloidal dispersions, and show high biocompatibility, leading to applications as biomarkers for in vitro and in vivo applications [59, 60]. The luminescence of the nanoparticles is determined by the anionic dye and can therefore show luminescence chromaticities in the whole visible spectral region. The ZrO-based nanoparticles used in this work both show green luminescence and were already thoroughly characterized [59, 60]. We chose these particles to ensure a distinction by luminescence chromaticity between the red-emitting Eu^{3+}-based MOF and the nanoparticle-based fluorophore. Furthermore, MFP-based particles were used to examine a dependence of the chromaticity on different solvents, since fluorescein-based chromophores show a strong solvatochromic effect [61]. The used nanoparticles ZrO(FMN) and ZrO(MFP) and their respective luminescence properties are depicted in Figure 1.

As the second emissive component, we selected the luminescent MOF $^{3}_{\infty}[Eu_2(BDC)_3]\cdot 2DMF\cdot 2H_2O$ (EuBDC) [54–56]. Besides its highly intensive Eu^{3+}-4f-based emission in the red wavelength region, this MOF shows high moisture- and air-stability and stability toward all solvents that were applied as dispersion media (pyridine, THF, toluene). Here, we utilized the MOF for further functionalization of the nanoparticles in different solvents. Lanthanide-containing MOFs that are based on trivalent lanthanide ions can show luminescence and intense emission properties that are based on a sensitizer effect of the MOF linker followed by emission based on the 4*f*–4*f* transitions of Ln^{3+} [62]. In our case, the parity-forbidden nature of these transitions can be overcome by excitation of the organic ligand BDC^{2-} that acts as a sensitizer and transfers its energy to the Ln^{3+} ion [62, 63].

We were able to use ZrO(FMN) and ZrO(MFP) nanoparticles as a basis for luminescent $LnCl_3$-modified composite particles and for pH-dependent optical sensing in the past [64, 65]. Additionally, the MOF EuBDC was used as luminescent compound for the preparation of different luminomagnetic microscale composite materials based on Fe_3O_4/SiO_2 composite particles [20, 66]. Further developing these results, we now used a solvothermal approach for the functionalization of ZrO-based nanoparticles with the MOF EuBDC. In principle, different ratios of both components can be combined. As the emission intensity of the MOF is much stronger than that of the two fluorophore nanoparticle systems, a 1:1 stoichiometric ratio is dominated by the Eu-based emission. For the FMN-containing composite material $^{3}_{\infty}[Eu_2(BDC)_3]\cdot 2DMF\cdot 2H_2O$@ZrO(FMN) (**1**, EuBDC@ZrO(FMN)), therefore, we used a ratio of ZrO(FMN):EuBDC of 5:1 to obtain a similar intensity of the luminescence processes of both compounds. The reaction was performed under solvothermal conditions in pyridine at 180 °C. The second luminescent composite material $^{3}_{\infty}[Eu_2(BDC)_3]\cdot 2DMF\cdot 2H_2O$@ZrO(MFP) (**2**, EuBDC@ZrO(MFP)) was successfully prepared at room temperature in toluene and THF as dispersion media.

Although the porosity of the MOF system is utilized for the interaction of the composites with solvents, EuBDC was not activated before or after composite formation, because for the dual emission, the materials are not used in a porous form, as the photophysical properties, including the solvatochromic effects, rely on filled pores.

2.1 | Properties of EuBDC@ZrO(FMN) (1)

The composite material EuBDC@ZrO(FMN) (**1**) as a dispersion in pyridine shows intensive luminescence properties upon excitation via UV light that can be varied depending on the excitation wavelength in terms of the luminescence chromaticity. While excitation with λ_{exc} = 300 nm results in red luminescence, excitation wavelength of λ_{exc} = 365 nm results in green luminescence. This property can be explained by the two-component character of the composite material: The green emission is based on the nanoparticle chromophore ZrO(FMN), while the MOF component Eu(BDC) shows a red luminescence chromaticity of 4f-based Eu^{3+}-emission, as described before. Since both emission processes exhibit different excitation ranges, the resulting emission can in principle be decoupled to a dual emission and chromaticity being excitation dependent. One of the two emission processes is dominating so that only a very weak modification of the luminescence of the single components is observed. The luminescence spectra and corresponding chromaticity of **1** are depicted for different excitation wavelengths in Figure 2.

For an excitation wavelength of λ_{exc} = 300 nm, the emission spectrum is dominated by the sharp 4*f*–4*f* transitions of Eu^{3+}. For EuBDC, the transition $^5D_0 \rightarrow {}^7F_2$ exhibits the highest intensity due to the centrosymmetric surrounding of the Eu^{3+} ion [61, 67]. This transition is hypersensitive, i.e., it depends on the local symmetry of the lanthanide ion and the dipole moment of the referring

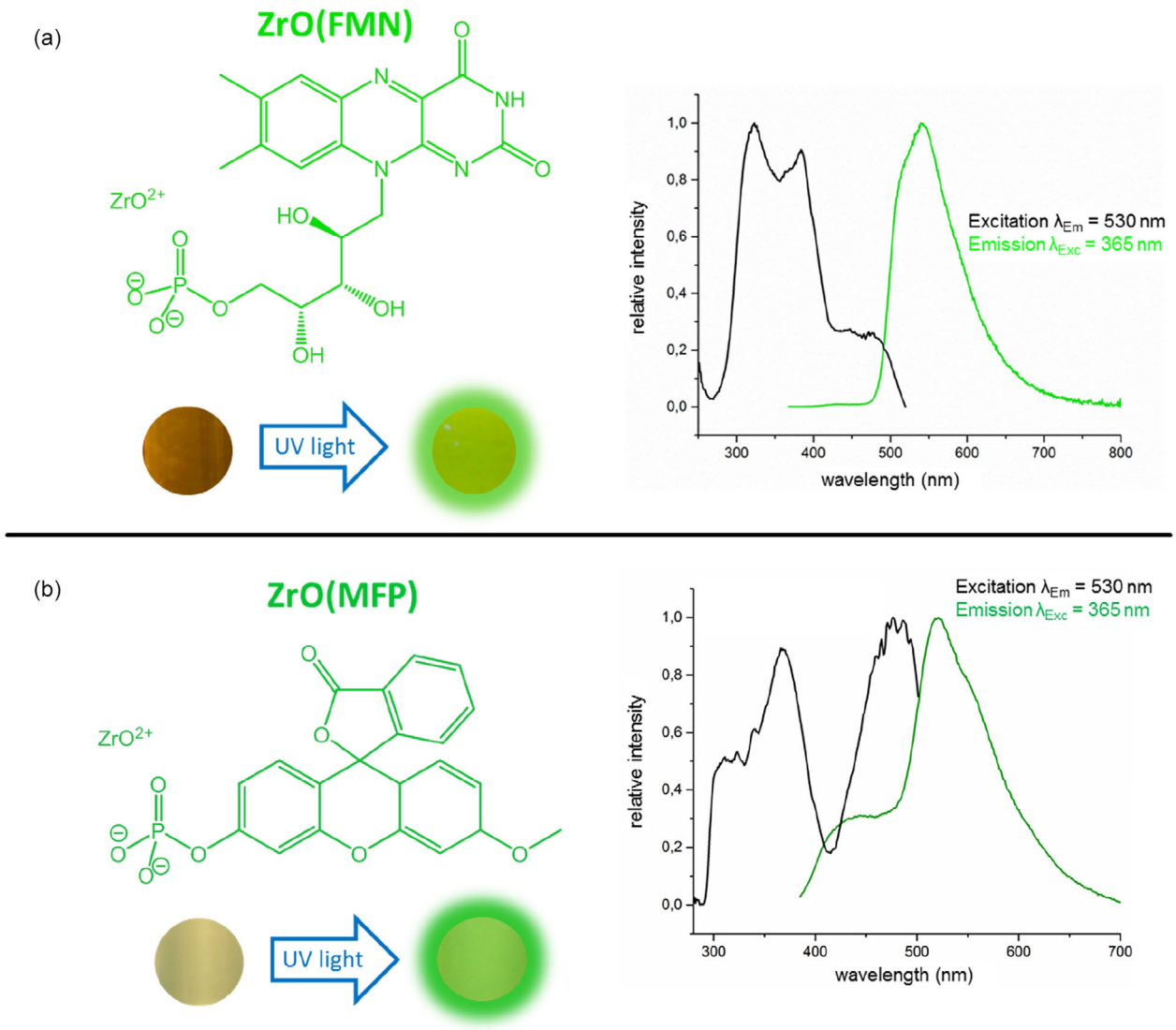

FIGURE 1 | Composition and constituents (left) as well as referring emission and (a) excitation spectra (right) of ZrO(FMN) and (b) ZrO(MFP).

transition (see also Figures S1 and S2 for more detailed depictions of the spectra and Figure S13 for a Jablonski diagram of the relevant photophysical processes of the components and composites) [68, 69]. The antenna effect of the BDC^{2-} anion is visible in the excitation spectrum by an excitation band with $\lambda_{max} = 302$ nm that reaches up to a wavelength of 330 nm. Additionally, weak direct 4*f*–4*f* excitation of Eu^{3+} can be observed at 394 nm with significantly lower intensity than the ligand excitation. The nanoparticle fluorescence of ZrO(FMN) can be excited over a broad UV region with a maximum at $\lambda_{max} = 350$ nm. However, the intensity of the ZrO(FMN) emission for $\lambda_{exc} < 330$ nm is significantly lower than the MOF emission and, thus, the emission spectrum is dominated by the red Eu^{3+}-emission.

For excitation wavelengths $\lambda_{exc} > 330$ nm, both luminescence processes can be observed, but the nanoparticle fluorescence is significantly more intense so that green chromaticity results originating from the nanoparticle fluorescence. Excitation of **1** with $\lambda_{exc} = 365$ nm leads to a broad band emission with $\lambda_{max} = 540$ nm that can be assigned to the FMN fluorophore. Compared to the unmodified ZrO(FMN) particles, the emission maximum shows a bathochromic shift of 10 nm. This indicates an interaction of the fluorophore with the Lewis acidic Eu^{3+} ions of the MOF, possibly by interaction with the functional groups of the nanoparticles (see Figure 1). The existence of the Eu^{3+} luminescence outside of the excitation range of the BDC^{2-} ligand indicates a sensitizer effect of the FMN chromophore by an energy transfer from the excited states of the nanoparticles to excited 4f-states after connection to the Eu^{3+} ions without an energy exchange of BDC^{2-} and FMN. The antenna effect of FMN is significantly weaker than the energy transfer of BDC^{2-}, which causes a lower intensity of the Eu^{3+} emission for higher excitation wavelengths ($\lambda_{exc} > 330$ nm). Thus, the Eu^{3+} excitation occurs by two different mechanisms for the different excitation wavelengths. Since the 4*f*–4*f* transitions of Eu^{3+} show a narrow band character, they comprise a smaller wavelength region than the broad band luminescence of ZrO(FMN) and therefore show only a weak influence on the resulting chromaticity of the composite so that the chromaticity of the composite can also be green with additional emission from Eu^{3+}-states showing a mixed color like other composite materials with different luminescence processes [70, 71]. This energy transfer is also indirect proof for the

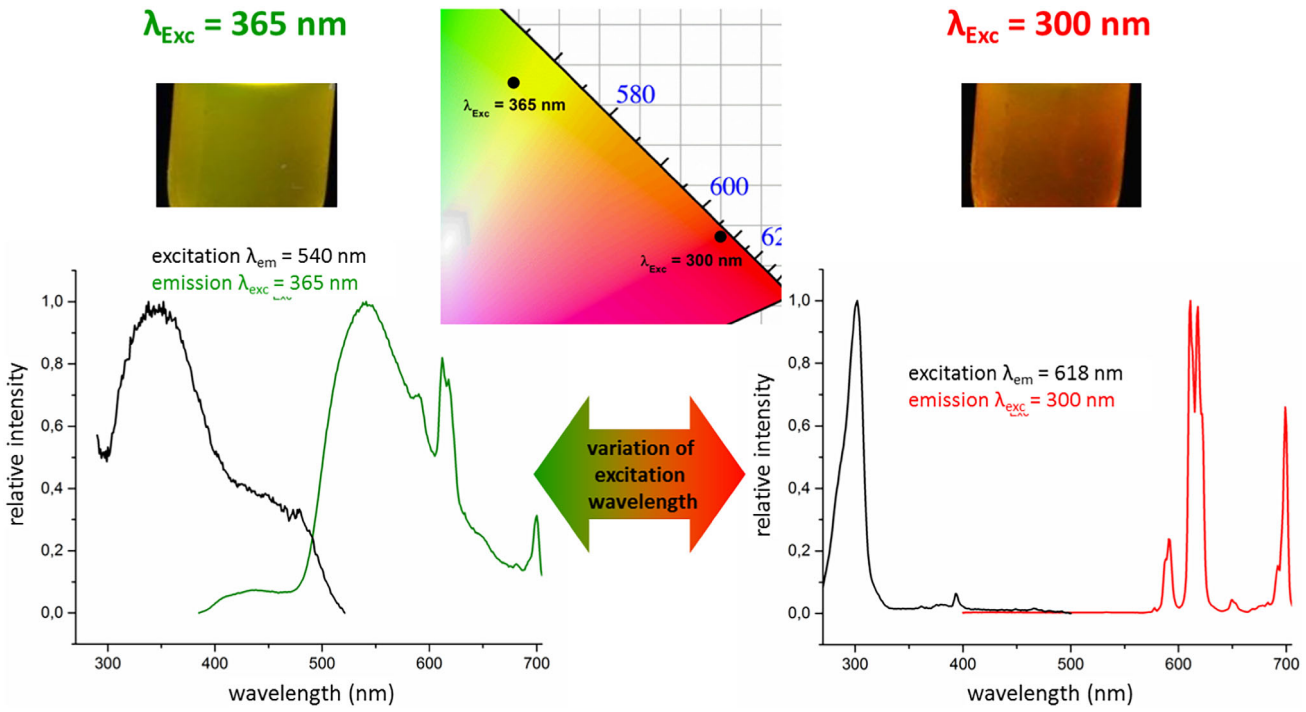

FIGURE 2 | Excitation and emission spectra as well as chromaticity of the composite system EuBDC@ZrO(FMN) (**1**) in pyridine for different excitation wavelengths (λ_{exc} = 365 nm (left), λ_{exc} = 300 nm (right)) and excerpt of the CIE diagram with resulting color points (center).

formation of a composite material. No opposite energy transfer from excited states of the MOF components to the ZrO(FMN) particles is observed for an excitation of the MOF at λ_{exc} = 300 nm.

Therefore, the composite EuBDC@ZrO(FMN) (**1**) combines two different luminescence processes that are reversibly selectable by variation of the excitation energy. The material exhibits an easily readable chromaticity difference of the emission between green and red and, hence, shows a remarkable potential for application as optically switchable material, which is fast, as it does not require a chemical transformation for the dual emission.

In order to further characterize the luminescence properties of composite **1**, luminescence lifetime measurements by determination of the overall process decay time were executed (see Table S1). For the emission of the nanoparticle fluorophore (λ_{exc} = 365 nm, λ_{em} = 540 nm), a bi-exponential decay with τ_1 = 4.4 ns and τ_2 = 7.0 ns could be calculated. Thus, the lifetime is slightly shorter than for the unmodified fluorophore FMN ($\tau \approx 5$ ns) [72, 73], indicating a weak influence of energy transfer to the Eu^{3+}-containing MOF on the π-system of the fluorophore. The lifetime of the 4*f*–4*f* transitions of Eu^{3+} (λ_{exc} = 300 nm, λ_{em} = 618 nm) can also be described by a bi-exponential fit with significantly longer lifetimes of τ_1 = 0.4 ms and τ_2 = 1.2 ms. The long lifetime is reasonable due to the parity forbiddance of the 4*f*–4*f* transitions and coincides well with the lifetimes of reported Eu^{3+}-based luminescent compounds, such as coordination polymers [74, 75].

For further characterization of composite material **1**, the dispersion in pyridine was evaporated and the dried material analyzed via SEM/EDX, elemental analysis, powder X-ray diffractometry and IR spectroscopy. Characterization via electron microscopy of the MOF-functionalized system **1** shows the formation of aggregates of different sizes, which show a diameter up to 15 µm (see Figure S3). The agglomeration of the nanoparticles to microparticles after modification with a Ln-containing compound could already be observed for the functionalization of ZrO(FMN) with $LnCl_3$ in a previous work [64, 65].

The distribution of the single components and therefore the homogeneity of the composite material was analyzed via an EDX mapping. Figure 3 shows the distribution of the elements Zr, P, Eu, and O in the composite material EuBDC@ZrO(FMN) (**1**). All elements can be detected in the complete examined region of the sample, but show varying concentrations of the single elements in different areas of the material. Spots with a high Eu concentration can be assigned to a high modification of the ZrO(FMN) with the MOF component. The concentration of O in the composite remains nearly unaltered in the whole examined region, since O can be detected in the carboxylate-based MOF as well as in the zirconyl- and phosphate-containing nanoparticles.

The element ratio detected via EDX shows a higher amount of the nanoparticle elements Zr and P in comparison with Eu (see Table S2). The detected Zr:Eu ratio of 3:1 can be assigned to a ratio ZrO(FMN):EuBDC of 6:1 based on the chemical formulas, and the latter values coincide with the ratio of substances used for the synthesis (ZrO(FMN):EuBDC = 5:1, as chosen to reach an equal intensity of the dual emission). The ratio of both components can be further confirmed via elemental analysis. The amounts of C, H, and N can be assigned to a ratio ZrO(FMN):EuBDC of 5:1 and are therefore in accordance with the EDX investigations.

The identity of the MOF component $^3{}_\infty[Eu_2(BDC)_3]\cdot 2DMF\cdot 2H_2O$ (EuBDC) was also investigated by powder X-ray diffraction

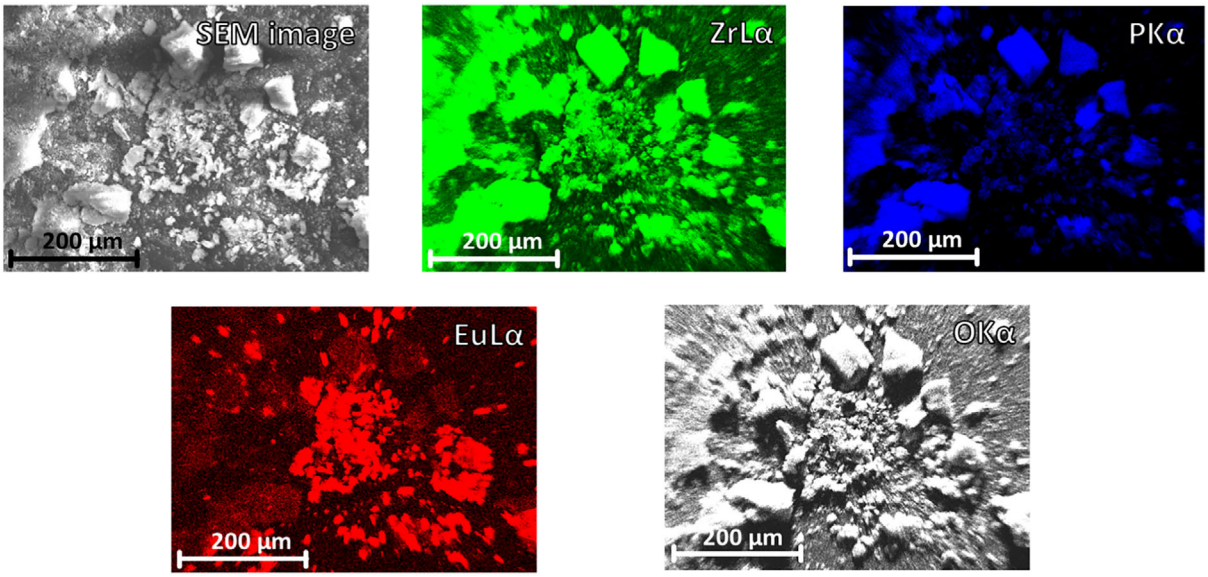

FIGURE 3 | SEM images and corresponding EDX element mapping of dried EuBDC@ZrO(FMN) (**1**) for the elements Zr, P, Eu, and O.

(PXRD) analysis of the dried composite particles **1** (see Figure S4). The resulting composite shows reduced crystallinity of the MOF, whereas the fluorophore particles are noncrystalline. The composite material shows similar reflection positions to EuBDC, such as the main reflection of the MOF at $2\theta = 9.7°$ and significant reflections at $2\theta = 9.1°$, 10.4°, 10.9°, and 18.9°. However, some intensities differ, as, e.g., the MOF reflection at $2\theta = 9.1°$ shows a significantly higher intensity in the composite material in relation to the other reflections, while the reflection at $2\theta = 15.6°$, being of high intensity in EuBDC, can hardly be detected in **1**. As a result, the identity of EuBDC can be confirmed with minor variation of the PXRD pattern, hinting at partial exchange of the solvent molecules water and DMF by pyridine, or at possible preferred orientation of the crystallites that could be assigned to a preferred orientation of the MOF layer during the composite formation.

IR spectroscopic investigations of **1** show the vibration bands typical for the FMN chromophore, such as the P—O vibration of the phosphate group (1008 cm^{-1}) or the C=C deformation vibration of the aromatic systems (1709 cm^{-1}) (see Figure S5). The harmonic C=O vibration of the carbonyl groups (3420 cm^{-1}) and the O—H vibration (3500 cm^{-1}) of the nanoparticles show a weaker intensity in the composite material, indicating interaction of the MOF components with the oxo and hydroxyl groups of the nanoparticles.

2.2 | Properties of EuBDC@ZrO(MFP) (2)

The composite material EuBDC@ZrO(MFP) (**2**) also shows intensive luminescence properties that differ depending on the excitation wavelength and the applied solvent. In analogy to **1**, the luminescence properties are dominated by the 4f-based Eu^{3+}-emission for $\lambda_{exc} = 300$ nm and by the MFP fluorescence for $\lambda_{exc} = 365$ nm. This results in different chromaticities of the composite that are reversibly switchable by variation of the excitation wavelength. Again, dual emission by applying different excitation energies is observed without the need for a chemical transformation. The respective photophysical processes described for **1** also apply for **2**. However, composite material **2** also shows some distinct differences to **1**.

In contrast to the ZrO(FMN)-based composite **1**, the EuBDC-functionalized ZrO(MFP) nanoparticles **2** show distinctively less emission of Eu^{3+} for higher excitation wavelengths and, thus, hardly any energy transfer from the zirconyl fluorophore to the MOF and excited states of Eu^{3+} leading to a stronger separation into dual emission of either the fluorophore or of the MOF EuBDC (Figure 4; see also Figures S6–S9 for more detailed depictions). Contrary to the FMN-based composite **1**, for $\lambda_{exc} = 365$ nm in the MFP-containing composite **2**, only the most intensive transition $^5D_0 \rightarrow {}^7F_2$ ($\lambda_{max} = 614$ nm) can be detected in the emission spectra. Hence, the energy transfer from excited states of FMN to the metal ion is more effective than for MFP as sensitizer, which results in a more intensive Eu^{3+} emission for **1** outside of the excitation range of BDC^{2-}.

In addition, with **2**, dual emission dispersions were successfully prepared with different solvents as dispersion media. Depending on the dispersion media, further chromaticity changes are induced by an intensive solvatochromic effect that leads to different chromaticities of **2** in toluene (nonpolar) and THF (polar). It is known that fluorescein-based luminophores can exhibit a strong dependence of their luminescence properties on the solvent that is caused by the strength of the hydrogen bonding between solvent and chromophore as well as by the polarity of the solvent [76, 77]. The MFP- and EuBDC-containing composite **2** combines dual emission and luminescence switching due to the two-component character of the system with the solvatochromic effect of ZrO(MFP). The different chromaticities as well as the corresponding excitation and emission spectra of **2** in THF and toluene are depicted in Figure 4. The solvatochromic effect of MFP is even visible for excitation wavelengths with higher energy ($\lambda_{exc} = 300$ nm), because the nanoparticles can still be excited in this region. This results in an orange luminescence

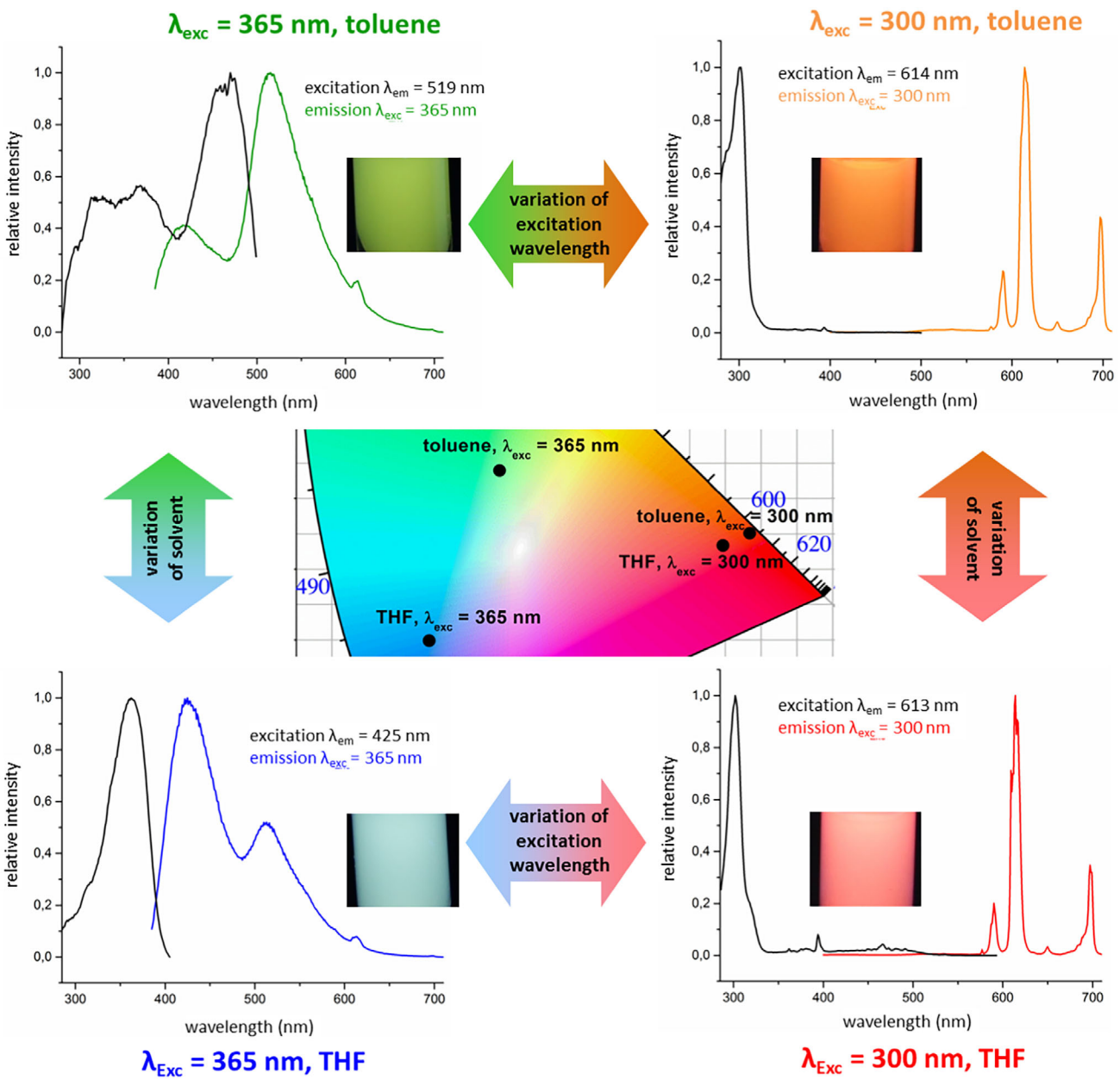

FIGURE 4 | Excitation and emission spectra as well as chromaticity of the composite system EuBDC@ZrO(MFP) (**2**) in toluene (top) and THF (bottom) for different excitation wavelengths (λ_{exc} = 365 nm (left), λ_{exc} = 300 nm (right) and excerpt of the CIE diagram with resulting color points (center).

of composite **2** in a dispersion of toluene with λ_{exc} = 300 nm that can be shifted to the green spectral region by variation of the excitation wavelength to λ_{exc} = 365 nm.

A dispersion of the composite material in THF shows a bright pink luminescence chromaticity for λ_{exc} = 300 nm, and instead of green, a light blue chromaticity for excitation at λ_{exc} = 365 nm.

Thereby, the ZrO(MFP) nanoparticles show a broad emission band with two local maxima. While one of the maxima is observed in the green spectral region, the other one can be detected in the blue wavelength region. Both emission maxima show identical excitation bands and are therefore assignable to the excitation of the singlet state of the fluorophore. The relative intensity of both maxima is heavily influenced by the particular solvent. For an excitation wavelength of λ_{exc} = 365 nm, **2** shows an absolute emission maximum at λ_{max} = 515 nm in toluene and a further secondary emission band with λ_{max} = 425 nm, whereas in THF the absolute emission maximum is at λ_{max} = 416 nm with a secondary emission maximum at 520 nm. While the band in the green region exhibits the 2.5-fold intensity of the blue emission for toluene, in THF, the blue emission at higher energies is two times more intensive than the green emission band. This results in a green luminescence chromaticity of the particles in toluene and blue in THF (λ_{exc} = 365 nm).

The ability of a solvent to form hydrogen bonds with the chromophore results in a shift of the excitation and emission spectra. Since the ZrO(MFP) nanoparticles were synthesized in water, the chromophore will likely be present in its protonated form [59].

THF can act as a Brønstedt base and form hydrogen bonds with the chromophore, while toluene does not form hydrogen bonds with the MFP fluorophore unit. Accordingly, fluorescein shows a significant blue shift for solvents that are able to form hydrogen bonds [78], which explains the different luminescence properties of the composite EuBDC@ZrO(MFP) (**2**) in toluene and THF.

For composite **2**, the described solvatochromic effect can be combined with the switchability to the red emission of the Eu^{3+}-containing MOF component by variation of the excitation wavelength. Though the nanoparticle emission shows a significantly weaker intensity than the Eu^{3+} emission bands for λ_{exc} = 300 nm, it nevertheless can influence the resulting chromaticity. In THF, the nanoparticle fluorescence causes a small blue shift of the emission band, resulting in a pink chromaticity of the composite. In contrast, the luminescence is shifted toward the green spectral region in toluene, resulting in an orange luminescence chromaticity. The relative intensities of the Eu^{3+} emission are identical in both solvents. Therefore, only the solvatochromic effect of the organic fluorophore is responsible for the different luminescence chromaticities in THF and toluene at λ_{exc} = 300 nm.

Luminescence lifetimes of the MFP-based composite **2** were also determined and can be calculated with a bi- or a tri-exponential decay, the latter with τ_1 = 0.7 ns, τ_2 = 3.2 ns, and τ_3 = 11.2 ns for the MFP emission bands (λ_{exc} = 365 nm, λ_{em} = 420, 540 nm) (see Table S3). Both emission maxima show the same lifetimes and coincide with the fluorescence lifetime of fluorescein (τ = 4.1 ns) [79]. Since both emission maxima show the same lifetimes, it can be confirmed that both bands are assignable to the MFP fluorescence process. The Eu^{3+} emission of the MOF component (λ_{exc} = 300 nm, λ_{em} = 615 nm) was calculated with a bi-exponential decay and lifetimes of τ_1 = 0.5 ms, τ_2 = 1.2 ms. These values are in good accordance with the lifetimes of composite **1** as well as with Eu^{3+}-containing coordination polymers [74, 75]. Also, see Figure S13 for a Jablonski diagram of the relevant photophysical processes.

To characterize the chromaticity dependence of the switchable emission of **2** on the particular excitation wavelength more deliberately, emission spectra of the composite dispersed in THF were recorded within an excitation range between 300 and 370 nm with stepwise variation of the excitation wavelength (step width 1 nm). Selected excitation and emission spectra in dependence on the excitation wavelength and the resulting color points are depicted in Figure 5 for a step width of 5 nm.

The respective detailed photoluminescence spectroscopy investigation of **2** in THF shows that an increasing excitation wavelength leads to a continuous decrease of the Eu^{3+} emission as well as to an increase of the intensity of the MFP emission (see Figure 5b and Figure S10 for more details). This results in a blue chromaticity shift of the luminescence with increasing excitation wavelength (see Figure 5c). It is obvious that the main color change occurs in the excitation wavelength region between 300 and 325 nm. A further increase of the excitation wavelength leads only to a minor blue shift of the luminescence. This phenomenon can be explained by analyzing the intensity progression of the excitation spectra for the Eu^{3+} and the MFP emission (see Figure 5a). The broad excitation band of the BDC^{2-} ligand as sensitizer for the Eu^{3+} emission (λ_{em} = 615 nm) shows an excitation maximum at λ_{max} = 300 nm and a strong decrease in the region of

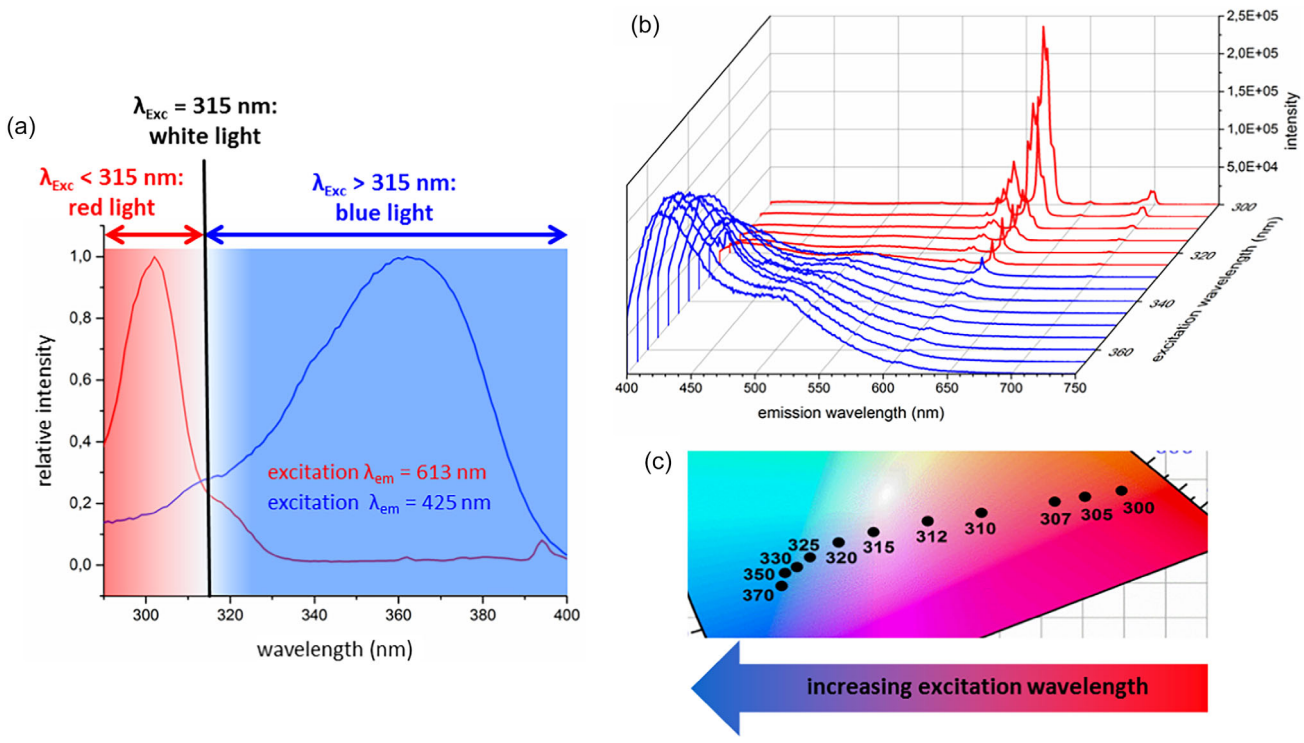

FIGURE 5 | (a) Excitation wavelength dependent luminescence properties of the composite EuBDC@ZrO(MFP) (**2**) in THF: Excitation spectra for the two different emission maxima with marked chromaticity regions of the emission, (b) emission spectra in dependence on the excitation wavelength (λ_{exc} = 300–370 nm), and (c) excerpt of the CIE diagram with resulting color points in dependence on the excitation wavelength.

305–325 nm. The excitation band of the blue MFP fluorescence (λ_{em} = 425 nm) increases in the whole excitation region up to λ_{max} = 370 nm. From 325 nm on, the 4*f*–4*f* transitions of Eu^{3+} show rather weak intensity and have only a minor influence on the resulting chromaticity, leading to blue luminescence. Therefore, the complete chromaticity change between red and blue takes place between excitation wavelengths of 305 and 325 nm and proceeds along the line of purples of the CIE diagram. The chromaticity change occurs continuously in the region of 300–325 nm. This enables a highly sensitive determination of the excitation wavelength by means of the chromaticity of the composite particles.

At the intersection of both excitation spectra (λ_{exc} = 315 nm), the red emission of Eu^{3+} and the blue luminescence of the nanoparticles are weighted similarly and add up to a chromaticity (x = 0.29, y = 0.29) in the proximity of ideal white point of the visible spectrum (x = 0.33, y = 0.33). Furthermore, upon excitation at λ_{exc} = 315 nm, the luminescence of composite **2** shows a very high color rendering index of 99, which is significantly higher than the CRIs of established illuminants [80].

For the structural characterization of **2**, the particle dispersion in THF was evaporated and analyzed via scanning electron microscopy (SEM), PXRD, and IR spectroscopy. In analogy to composite **1**, electron microscopic investigations of the dried particles show an aggregation of the nanoparticles to microparticles after removal of the solvent (see Figure S11). The resulting agglomerates show particle sizes of 1–10 µm.

PXRD analysis shows a broad intensity region in the diffractogram that indicates a high amorphous content of the sample (see Figure S12). This background was also detectable for the unmodified ZrO(MFP) particles and is assignable to residues that could not be removed even under vacuum and at high temperatures (T = 150 °C). This was also evident by the high viscosity of the sample. Despite the high amorphic character of the particles, crystalline amounts could also be detected in composite **2** that confirm the identity of the MOF $^{3}_{\infty}[Eu_2(BDC)_3]\cdot 2DMF\cdot 2H_2O$ (EuBDC) by the main reflections of EuBDC being detectable at 2θ = 15.9° and 24.4°.

IR spectroscopy was used to confirm the presence of the ZrO(MFP) nanoparticles in the composite. This is evident by the P—O vibration of the phosphate group (1008 cm^{-1}) and the C=C deformation vibrations (1258 cm^{-1}, 787 cm^{-1}). Furthermore, the C—H stretching vibration of THF (3000 cm^{-1}) can be detected and confirms, together with the previous analytical methods, the presence of residues of the solvent in the composite material.

3 | Conclusion

Functionalization of luminescent zirconyl-based nanoparticles with the luminescent Eu^{3+} containing MOF EuBDC leads to preparation of the multi-luminescent composite materials EuBDC@ZrO(FMN) (**1**) and EuBDC@ZrO(MFP) (**2**). These materials form particle composites that allow for dual emission of light. Both materials combine two different luminescence processes that show distinct differences in terms of their emission chromaticity and their excitation energy. By variation of the excitation wavelength, optical switching of the chromaticity of the composite materials can be enabled without a chemical transformation being required for the dual emission. Therefore, both materials show significant potential as sensitive and reversible optical switches and an "on-the-fly"-detectable emission color difference. While the FMN-based material **1** is variable between the red and green spectral region, the MFP-containing composite **2** complements the switchability by a strong solvatochromic effect of the nanoparticle compound. Therefore, an even higher variety of the resulting chromaticity can be accessed. Based on the polarity of the solvent, variation of the excitation wavelength can lead to a solvatochromic chromaticity shift from orange to green in toluene and from pink to blue in THF. Scaling of the chromaticity change enables calculation of the excitation wavelength by the chromaticity point according to CIE. Additionally, EuBDC@ZrO(MFP) can be run close to a white light emitter with a high CRI under certain excitation conditions.

4 | Experimental Section

4.1 | Synthetic Procedures

4.1.1 | *Reagents*

ZrO(FMN) and ZrO(MFP) were prepared according to references [59] and [60] by reaction of an aqueous solution of $ZrOCl_2\cdot 8H_2O$ with sodium riboflavin-5′-monophosphate dihydrate and cyclohexylammonium methylfluorescein phosphate, respectively. After synthesis, ZrO(FMN) particles were dispersed in pyridine, and ZrO(MFP) particles were dispersed in THF and toluene, respectively. Nitric acid (Otto Fischar GmbH & Co. KG), terephthalic acid (abcr, 98%), and Eu_2O_3 (99%, Research Chemicals) were used without further purification.

4.1.2 | *Synthesis of $^{3}_{\infty}[Eu_2(BDC)_3]\cdot 2DMF\cdot 2H_2O$ (EuBDC)*

$Eu(NO_3)_3\cdot 5H_2O$ was synthesized prior to the MOF synthesis according to ref. [81] by dissolving Eu_2O_3 in 6 M nitric acid and subsequent removal of the solvent under vacuum at 100 °C. Na_2BDC was synthesized according to reference [82] by reaction of NaOH with terephthalic acid (H_2BDC). The MOF $^{3}_{\infty}[Eu_2(BDC)_3]\cdot 2DMF\cdot 2H_2O$ (EuBDC) was synthesized by reaction of Na_2BDC with $Eu(NO_3)_3\cdot 5H_2O$ in DMF/H_2O and subsequent removal of the solvent under vacuum according to reference [61].

4.1.3 | *Synthesis of $^{3}_{\infty}[Eu_2(BDC)_3]\cdot 2DMF\cdot 2H_2O$@ZrO(FMN) (1)*

$^{3}_{\infty}[Eu_2(BDC)_3]\cdot 2DMF\cdot 2H_2O$ (2.50 µmol, 2.45 mg) was placed together with 1.0 mL of a dispersion of ZrO(FMN) (12.5 µmol, 7.00 mg) in pyridine in a Duran glass ampoule and subsequently frozen with liquid nitrogen and degassed. After evacuation and sealing of the ampoule, the reaction mixture was heated up to 180 °C for 24 h. The dispersion was separated from the precipitate for analysis. The precipitate was dried under vacuum and prepared for the remaining analytical investigations.

Elemental analysis calculated for $Eu_2C_{115}H_{125}N_{22}O_{66}P_5Zr_5$ (=(EuBDC)(ZrO(FMN))$_5$) (M = 3778.43 g mol^{-1}): C: 35.56, H:3.33, N: 8.16%. Found: C: 36.52, H: 4.18, N: 9.07%. MIR: (3179 (w), 2924 (w), 2853 (w), 1709 (m), 1580 (w), 1546 (m), 1466 (w), 1357 (w), 1221 (w), 1008 (s), 997 (w)) cm^{-1}.

4.1.4 | *Synthesis of $^3_\infty$[Eu$_2$(BDC)$_3$]·2DMF·2H$_2$O@ZrO(MFP) (2)*

$^3_\infty$[Eu$_2$(BDC)$_3$]·2DMF·2H$_2$O (1.87 µmol, 1.83 mg) was placed together with 0.5 mL of a dispersion of ZrO(MFP) (1.87 µmol, 1.00 mg) in THF and toluene, respectively, in a round flask. The reaction mixture was stirred for 24 h at room temperature. The dispersion was prepared for photoluminescence analysis.

For further analytical investigations, $^3_\infty$[Eu$_2$(BDC)$_3$]·2DMF·2H$_2$O (37.6 µmol, 36.8 mg) and 10 mL of a dispersion of ZrO(MFP) (37.6 µmol, 20.0 mg) in THF were placed in a Schlenk flask and stirred at room temperature. The viscous reaction product could not be dried under vacuum at 150 °C.

MIR: (2963 (m), 1410 (w), 1258 (s), 1080 (m), 1008 (s), 849 (w), 787 (s), 728 (w) cm^{-1}.

4.2 | Analytical Investigations

4.2.1 | *Photoluminescence Spectroscopy*

Excitation and emission spectra were recorded using a Horiba Jobin Yvon Fluorolog 3 spectrometer with a 450 W Xe lamp, a FL-1073 photomultiplier tube detector, and Czerny–Turner double gratings (1200 grooves per mm) emission and excitation monochromators. An edge filter was used to block the 1st and 2nd harmonic oscillations of the light source. Excitation spectra were recorded from 250 nm to 520 nm and corrected for the spectral distribution of the lamp using a photodiode reference detector. Emission spectra were recorded from 380 nm to 800 nm and corrected for the spherical response of the monochromator and the detector using correction spectra provided by the manufacturer. All samples were investigated as dispersions in spectroscopically pure quartz glass cuvettes in front-face mode at room temperature.

4.2.2 | *Luminescence Lifetimes*

Lifetimes of the luminescence processes were determined by investigation of the overall process decay time using an Edinburgh Instruments FLS920 spectrometer. The samples were prepared as dispersions in spectroscopically pure quartz glass cuvettes. Decay times were recorded by time-correlated single photon counting (TCSPC) using a microsecond flashlamp with λ_{exc} = 300 nm for the Eu^{3+} emissions and a pulsed picosecond laser diode (λ_{exc} = 375 nm, 5 mW) for nanoparticle-based luminescence processes. The emission was collected at right angles to the excitation source, and a single-photon avalanche diode (SPAD) was used as a detector. The resulting intensity decays were calculated via a tail fit analysis procedure (Edinburgh F900 analysis software). The quality of the fit was confirmed by low χ^2 values ($\chi^2 < 1.3$).

4.2.3 | *PXRD*

Powder diffraction analysis was performed on a Bruker D8 Discover diffractometer with Da Vinci design equipped with a focusing Göbel mirror and a linear LynxEye detector. Powders were prepared by grinding with a mortar and placed on a low-background silicon wafer. All samples were measured in parallel beam geometry in reflection mode using CuK_α radiation (λ = 1.54056 Å).

4.2.4 | *SEM and Energy Dispersive X-Ray Spectroscopy (EDX)*

The surface structure of the composite materials was investigated using a field emission scanning electron microscope (FE-SEM) Ultra plus (Zeiss) with a GEMINI e-beam column and a Schottky emitter. Elemental analysis and mapping were carried out via EDX using a silicon drift detector (SDD) X-Max 50 mm^2 (Oxford Instruments) at 20 keV for all composite materials. Samples were prepared on a self-adhesive graphite patch.

4.2.5 | *IR Spectroscopy*

IR spectra were recorded over the range from 4000 to 700 cm^{-1} using a Nicolet 830 FT-IR spectrometer in transmission mode and the software OMNIC 32.

4.2.6 | *Elemental Analysis*

CHN analysis was carried out on a Vario micro cube (Elementar Analysensysteme GmbH).

Acknowledgments

The authors gratefully acknowledge support of the *Deutsche Forschungsgemeinschaft* within the project FL-Detect (Grant No. MU-1562/19-1 and FE-911/17-1).

Open Access funding enabled and organized by Projekt DEAL.

Funding

This work was supported by Deutsche Forschungsgemeinschaft (Grants MU-1562/19-1, FE-911/17-1).

Conflicts of Interest

The authors declare no conflicts of interest.

Data Availability Statement

The data that supports the findings of this study are available in the supplementary material of this article.

References

1. F. D. Jochum and P. Theato, "Temperature and Light-Responsive Smart Polymer Materials," *Chemical Society Reviews* 42 (2013): 7468–7483.

2. F. Mumtaz, M. Faraz, H. K. Balakrishnan, R. Nair, and L. F. Dumée, "Stimuli-Responsive Membranes—Mechanisms, Materials and Future Directions," *Npj Clean Water* 9 (2026): 1.

3. Q. Zhang, Y. Zhang, Y. Wan, W. Carvalho, L. Hu, and M. J. Serpe, "Stimuli-Responsive Polymers for Sensing and Reacting to Environmental Conditions," *Progress in Polymer Science* 116 (2021): 101386.

4. A. Teixeira do Nascimento, P. R. Stoddart, T. Goris, et al., "Stimuli-Responsive Materials for Biomedical Applications," *Advanced Materials* 37 (2025): 07559.

5. S. Uredat, D. Truzzolillo, A. Gujare, J. Runge, J. Oberdisse, and T. Hellweg, "A Review of Stimuli-Responsive Polymer-Based Gating Membranes," *Physical Chemistry Chemical Physics* 26 (2024): 2732–2744.

6. M. A. C. Stuart, W. T. S. Huck, J. Genzer, et al., "Emerging Applications of Stimuli-Responsive Polymer Materials," *Nature Materials* 9 (2010): 101.

7. D. Roy, J. N. Cambre, and B. S. Sumerlin, "Future Perspectives and Recent Advances in Stimuli-Responsive Materials," *Progress in Polymer Science* 35 (2010): 278–301.

8. M. W. Urban, "Stratification, Stimuli-Responsiveness, Self-Healing, and Signaling in Polymer Networks," *Progress in Polymer Science* 34 (2009): 679–687.

9. M. Karg and T. Hellweg, "Smart Inorganic/Organic Hybrid Microgels: Synthesis and Characterisation," *Journal of Materials Chemistry* 19 (2009): 8714–8727.

10. M. Suta, "What makes β-$NaYF_4$:Er^{3+},Yb^{3+} Such a Successful Luminescent Thermometer?," *Nanoscale* 17 (2025): 7091–7099.

11. J. D. Debord and L. A. Lyon, "Thermoresponsive Photonic Crystals," *The Journal of Physical Chemistry B* 104 (2000): 6327–6331.

12. I. Dimitrov, B. Trzebicka, A. H. E. Müller, A. Dworak, and C. B. Tsvetanov, "Thermosensitive Water-Soluble Copolymers with Doubly Responsive Reversibly Interacting Entities," *Progress in Polymer Science* 32 (2007): 1275–1343.

13. A. M. Schmidt, "Thermoresponsive Magnetic Colloids," *Colloid and Polymer Science* 285 (2007): 953–966.

14. Q. Zhou, G. Ren, Y. Yang, et al., "Fluorescence Thermometers Involving Two Ranges of Temperature: Coordination Polymer and DMSP Embedding," *Inorganic Chemistry* 62 (2023): 16652–16658.

15. D. Chauhan and C. Maity, "A Light Responsive Single Amino Acid-based Supramolecular Hydrogel for Photo-Controlled Vitamin Release," *Materials Advances* 7 (2026): 175–186.

16. J. S. Katz and J. A. Burdick, "Light-Responsive Biomaterials: Development and Applications," *Macromolecular Bioscience* 10 (2010): 339–348.

17. M. Natali and S. Giordani, "Molecular Switches as Photocontrollable "smart" Receptors," *Chemical Society Reviews* 41 (2012): 4010–4029.

18. Y. Zhao," Photocontrollable Block Copolymer Micelles: What Can We Control?," *Journal of Materials Chemistry* 19 (2009): 4887–4895.

19. D. Fischer, L. V. Meyer, M. Jansen, and K. Müller-Buschbaum," Highly Luminescent Thin Films of the Dense Framework $^{3\infty}$[EuIm2] with Switchable Transparency Formed by Scanning Femtosecond-Pulse Laser Deposition," *Angewandte Chemie International Edition* 53 (2014): 706–710.

20. K. Mandel, T. Granath, T. Wehner, et al., "Smart Optical Composite Materials: Dispersions of Metal–Organic Framework@ Superparamagnetic Microrods for Switchable Isotropic–Anisotropic Optical Properties," *ACS Nano* 11 (2017): 779–787.

21. J. L. Funnell, A. M. Ziemba, J. F. Nowak, et al., "Assessing the Combination of Magnetic Field Stimulation, Iron Oxide Nanoparticles, and Aligned Electrospun Fibers for Promoting Neurite Outgrowth from Dorsal Root Ganglia in Vitro," *Acta Biomaterialia* 131 (2021): 302–313.

22. J. Ge, L. He, J. Goebl, and Y. Yin, "Assembly of Magnetically Tunable Photonic Crystals in Nonpolar Solvents," *Journal of the American Chemical Society* 131 (2009): 3484–3486.

23. C. Ederer and N. A. Spaldin, "A New Route to Magnetic Ferroelectrics," *Nature Materials* 3 (2004): 849.

24. Q. Yan, J. Yuan, Z. Cai, Y. Xin, Y. Kang, and Y. Yin, "Voltage-Responsive Vesicles Based on Orthogonal Assembly of Two Homopolymers," *Journal of the American Chemical Society* 132 (2010): 9268–9270.

25. D. Mandal, A. Sarkar, K. C. Behera, and M. Ravikanth, "pH-Responsive Supramolecular Switch of a Rationally Designed Dipyrroethene-Based Chromophore," *Chemical Science* 16 (2025): 1772–1782.

26. S. Dai, P. Ravi, and K. C. Tam, "pH-Responsive Polymers: Synthesis, Properties and Applications," *Soft Matter* 4 (2008): 435–449.

27. H. Patel, R. Singh, and B. Datta, "pH-Responsive Release of Small Molecule Pharmaceuticals from a Reworked Adsorbent Hydrogel for Environmental Applications," *RSC Advances* 15 (2025): 29462–29478.

28. G. Kocak, C. Tuncer, and V. Butun, *Polymer Chemistry* 8 (2017): 144–176.

29. D. Schmaljohann, "Thermo- and pH-Responsive Polymers in Drug Delivery," *Advanced Drug Delivery Reviews* 58 (2006): 1655–1670.

30. F. Ercole, T. P. Davis, and R. A. Evans, "Photo-Responsive Systems and Biomaterials: Photochromic Polymers, Light-Triggered Self-Assembly, Surface Modification, Fluorescence Modulation and beyond," *Polymer Chemistry* 1 (2010): 37–54.

31. C. B. Greenberg, "Optically switchable thin films: A Review," *Thin Solid Films* 251, 1994, 81–93.

32. H. Jinlian, M. Harper, L. Guoqiang, and I. Samuel, "A Review of Stimuli-Responsive Polymers for Smart Textile Applications," *Smart Materials & Structures* 21 (2012): 053001.

33. M. Andresen, A. C. Stiel, J. Folling, et al., "Photoswitchable Fluorescent Proteins Enable Monochromatic Multilabel Imaging and Dual Color Fluorescence Nanoscopy," *Nature Biotechnology* 26 (2008): 1035–1040.

34. D. M. Chudakov, V. V. Verkhusha, D. B. Staroverov, E. A. Souslova, S. Lukyanov, and K. A. Lukyanov, "Photoswitchable Cyan Fluorescent Protein for Protein Tracking," *Nature Biotechnology* 22 (2004): 1435–1439.

35. J. Wiedenmann, S. Ivanchenko, F. Oswald, et al., "EosFP, a Fluorescent Marker Protein with UV-Inducible Green-to-Red Fluorescence Conversion," *Proceedings of the National Academy of Sciences* 101 (2004): 15905–15910.

36. E. A. Jares-Erijman and T. M. Jovin, "FRET Imaging," *Nature Biotechnology* 21 (2003): 1387–1395.

37. A. Valentini, B. Dibnah, M. Ciba, et al., "Multicolored Sequential Resonance Energy Transfer for Detection of Simultaneous Ligand Binding at G Protein-Coupled Receptors," *Nature Communications* 16 (2025): 6413.

38. J. Xu, W. Ji, K. Zhu, et al., "Application of Fluorescence Resonance Energy Transfer in Homogeneous Immunoassay using Quantum Dots," *Coordination Chemistry Reviews* 542 (2025): 216872.

39. S. Li, B. Fu, H. Li, et al., "Eu-doped ZIF-8 as a Ratiometric Fluorescence-scattering Probe for the Anthrax Biomarker in Food Samples Based on Competitive Coordination," *Spectrochimica Acta Part A: Molecular and Biomolecular Spectroscopy* 307 (2024): 123642.

40. D. Lee, S. Khaja, J. C. Velasquez-Castano, et al., "In Vivo Imaging of Hydrogen Peroxide with Chemiluminescent Nanoparticles," *Nature Materials* 6 (2007): 765–769.

41. M. Irie, "Photochromism: Memories and Switches Introduction," *Chemical Reviews* 100 (2000): 1683–1684.

42. S. Kawata and Y. Kawata, "Three-Dimensional Optical Data Storage using Photochromic Materials," *Chemical Reviews* 100 (2000): 1777–1788.

43. M. Irie, T. Fukaminato, T. Sasaki, N. Tamai, and T. Kawai, "A Digital Fluorescent Molecular Photoswitch," *Nature* 420 (2002): 759–760.

44. A. P. de Silva, H. Q. N. Gunaratne, T. Gunnlaugsson, et al., "Signaling Recognition Events with Fluorescent Sensors and Switches," *Chemical Reviews* 97 (1997): 1515–1566.

45. J. Zhang, Q. Zou, and H. Tian, "Photochromic Materials: More Than Meets the Eye," *Advanced Materials* 25 (2012): 378–399.

46. M. Heilemann, E. Margeat, R. Kasper, M. Sauer, and P. Tinnefeld, "Carbocyanine Dyes as Efficient Reversible Single-Molecule Optical Switch," *Journal of the American Chemical Society* 127 (2005): 3801–3806.

47. M.-Q. Zhu, L. Zhu, J. J. Han, W. Wu, J. K. Hurst, and A. D. Q. Li, "Spiropyran-Based Photochromic Polymer Nanoparticles with Optically Switchable Luminescence," *Journal of the American Chemical Society* 128 (2006): 4303–4309.

48. J.-K. Sun, L.-X. Cai, Y.-J. Chen, Z.-H. Li, and J. Zhang, "Reversible Luminescence Switch in a Photochromic Metal–organic Framework," *Chemical Communications* 47 (2011): 6870–6872.

49. Z. Wang, Y. Ma, R. Zhang, et al., "Reversible Luminescent Switching in a $[Eu(SiW_{10}MoO_{39})_2]^{13-}$ -Agarose Composite Film by Photo-sensitive Intramolecular Energy Transfer," *Advanced Materials* 21 (2009): 1737–1741.

50. C. Carbonell, M. Linares-Moreau, S. M. Borisov, and P. Falcaro, "Multimaterial Digital-Light Processing of Metal-Organic Framework (MOF) Composites: A Versatile Tool for the Rapid Microfabrication of MOF-Based Devices," *Advanced Materials* 36 (2024): 2408770.

51. X. Wang, Y. Jiang, A. Tissot, and C. Serre, "Luminescent Sensing Platforms Based on Lanthanide Metal-Organic Frameworks: Current Strategies and Perspectives," *Coordination Chemistry Reviews* 497 (2023): 215454.

52. G. Gupta and A. Thakur," A Comprehensive Review on Luminescent Metal–Organic Framework Detectors," *Materials Today: Proceedings* 50 (2022): 1721–1725.

53. K. Müller-Buschbaum, F. Beuerle, and C. Feldmann, "MOF Based Luminescence Tuning and Chemical/Physical Sensing," *Microporous Mesoporous Materials* 216 (2015): 171–199.

54. Z.-H. Zhang, S.-Y. Wan, T.-a. Okamura, W.-Y. Sun, and N. Ueyama, "Synthesis and Crystal Structure of two Lanthanide Complexes with Benzenecarboxylic Derivatives," *Zeitschrift Fur Anorganische Und Allgemeine Chemie* 632 (2006): 679–683.

55. A. L. R. Talhari, F. G. M. Mauricio, B. R. B. Gomes, et al., "An Alternative Approach to the Detection of Latent Fingermarks Using $[Eu_2(BDC)_3(H2O)_2]$, a Luminescent Non-Toxic MOF Powder," *Journal of Forensic Sciences* 70 (2025): 531–549.

56. M. Maxeiner, R. Maile, M. Cuvalli, et al.," NanoMOF-Based Multilevel Anti-Counterfeiting by a Combination of Visible and Invisible Photoluminescence and Conductivity," *Advanced Functional Materials* 36 (2025): 2500794.

57. R. Ando, H. Mizuno, and A. Miyawaki, "Regulated Fast Nucleocytoplasmic Shuttling Observed by Reversible Protein Highlighting," *Science* 306 (2004): 1370.

58. I. L. Medintz, S. A. Trammell, H. Mattoussi, and J. M. Mauro, "Reversible Modulation of Quantum Dot Photoluminescence Using a Protein-Bound Photochromic Fluorescence Resonance Energy Transfer Acceptor," *Journal of the American Chemical Society* 126 (2004): 30–31.

59. M. Roming, H. Lünsdorf, K. E. J. Dittmar, and C. Feldmann, "$ZrO(HPO_4)_{1-x}$ $(FMN)_x$: Quick and Easy Synthesis of a Nanoscale Luminescent Biomarker," *Angewandte Chemie International Edition* 49 (2010): 632–637.

60. J. G. Heck, J. Napp, S. Simonato, et al., "Multifunctional Phosphate-Based Inorganic–Organic Hybrid Nanoparticles," *Journal of the American Chemical Society* 137 (2015): 7329–7336.

61. P. D. McQueen, S. Sagoo, H. Yao, and R. A. Jockusch, "On the Intrinsic Photophysics of Fluorescein," *Angewandte Chemie International Edition* 49 (2010): 9193–9196.

62. K. Binnemans, "Lanthanide-Based Luminescent Hybrid Materials," *Chemical Reviews* 109 (2009): 4283–4374.

63. J.-C. G. Bünzli and S. V. Eliseeva, *Springer Series on Fluorescence: Lanthanide Luminescence: Photophysical, Analytical and Biological Aspects* (Springer Verlag, 2011). 1–46, Vol. 7.

64. T. Wehner, J. Heck, C. Feldmann, and K. Müller-Buschbaum, "White Light Emission and Temperature Dependent Chromaticity Shifts by Modification of Luminescent ZrO (FMN) Nanoparticles with Rare Earth Halides," *Journal of Materials Chemistry C* 4 (2016): 7735–7743.

65. T. Wehner, J. Heck, C. Feldmann, and K. Müller-Buschbaum, "Reactivity of ZrO(MFP) and ZrO(RP) Nanoparticles with $LnCl_3$ for Solvatochromic Luminescence Modification and pH-Dependent Optical Sensing," *Chemistry–A European Journal* 25 (2019): 16630–16638.

66. T. Wehner, K. Mandel, M. Schneider, G. Sextl, and K. Müller-Buschbaum, "Superparamagnetic Luminescent MOF@Fe_3O_4/SiO_2 Composite Particles for Signal Augmentation by Magnetic Harvesting as Potential Water Detectors," *ACS Applied Materials & Interfaces* 8 (2016): 5445–5452.

67. Y. Han, X. Li, L. Li, et al., "Structures and Properties of Porous Coordination Polymers Based on Lanthanide Carboxylate Building Units," *Inorganic Chemistry* 49 (2010): 10781–10787.

68. K. Binnemans, "Interpretation of Europium(III) Spectra," *Coordination Chemistry Reviews* 295 (2015): 1–45.

69. G. Blasse, G. J. Dirksen, and F. Zonnevijlle, "The Luminescence of Some Lanthanide Decatung-States and Other Polytungstates," *Journal of Inorganic and Nuclear Chemistry* 43 (1981): 2847–2853.

70. T. Wehner, M. T. Seuffert, J. R. Sorg, et al., "Composite Materials Combining Multiple Luminescent MOFs and Superparamagnetic Microparticles for Ratiometric Water Detection," *Journal of Materials Chemistry C* 5 (2017): 10133–10142.

71. Y. Cui, H. Xu, Y. Yue, et al., "A Luminescent Mixed-Lanthanide Metal–Organic Framework Thermometer," *Journal of the American Chemical Society* 134 (2012): 3979–3982.

72. R. Leenders, M. Kooijman, A. van Hoek, C. Veeger, and A. J. W. G. Visser, "Flavin Dynamics in Reduced Flavodoxins," *European Journal of Biochemistry* 211 (1993): 37–45.

73. R. D. Spencer and G. Weber, "Measurements of Subnanosecond Fluorescence Lifetimes with a Cross-Correlation Phase Fluorometer," *Annals of the New York Academy of Sciences* 158 (1969): 361–376.

74. A. de Bettencourt-Dias, "Isophthalato-Based 2D Coordination Polymers of Eu(III), Gd(III), and Tb(III): Enhancement of the Terbium-Centered Luminescence through Thiophene Derivatization," *Inorganic Chemistry* 44 (2005): 2734–2741.

75. Y. Hasegawa, M. Yamamuro, Y. Wada, N. Kanehisa, Y. Kai, and S. Yanagida, "Luminescent Polymer Containing the Eu(III) Complex Having Fast Radiation Rate and High Emission Quantum Efficiency," *The Journal of Physical Chemistry A* 107 (2003): 1697–1702.

76. V. R. Batistela, J. da Costa Cedran, H. P. M. de Oliveira, et al., "Protolytic Fluorescein Species Evaluated Using Chemometry and DFT Studies," *Dyes and Pigments* 86 (2010): 15–24.

77. F. Naderi, A. Farajtabar, and F. Gharib, "Solvatochromic and Preferential Solvation of Fluorescein in Some Water-Alcoholic Mixed Solvents," *Journal of Molecular Liquids* 190 (2014): 126–132.

78. N. Klonis, A. H. A. Clayton, E. W. Voss, and W. H. Sawyer, "Spectral Properties of Fluorescein in Solvent-Water Mixtures: Applications as a Probe of Hydrogen Bonding Environments in Biological Systems," *Photochemistry and Photobiology* 67 (2008): 500–510.

79. D. Magde, G. E. Rojas, and P. G. Seybold, "Solvent Dependence of the Fluorescence Lifetimes of Xanthene Dyes," *Photochemistry and Photobiology* 70 (1999): 737–744.

80. A. J. Wilkins and C. Clark, "Modulation of Light from Fluorescent Lamps," *Lighting Research & Technology* 22 (1990): 103–109.

81. P. Bag, U. Florke, and K. Nag, "Synthesis and Structural Characterization of Lanthanide(III) Nitrate Complexes of a Tetraiminodiphenol Macrocycle in the Solid State and in Solution," *Dalton Transactions* 35 (2006): 3236–3248.

82. J. Kaduk, "Terephthalate Salts: Salts of Monopositive Cations," *Acta Crystallographica Section B Structural Science* 56 (2000): 474–485.

Supporting Information

Additional supporting information can be found online in the Supporting Information section.